

## Article

# Acetalization of Alkyl Alcohols with Benzaldehyde over Cesium Phosphomolybdo vanadate Salts

Márcio José da Silva <sup>1,\*</sup>, Cláudio Júnior Andrade Ribeiro <sup>2</sup>, Eduardo Nery de Araújo <sup>3</sup> and Isadora Merighi Torteloti <sup>1</sup>

<sup>1</sup> Chemistry Department, Federal University of Viçosa, Viçosa 36590-000, Brazil; isadora.tortelote@ufv.br

<sup>2</sup> Chemistry Department, Federal Institute of Education, Science and Technology of Minas Gerais, Pouso Alegre 37550-000, Brazil; claudio.ribeiro@ifmg.edu.br

<sup>3</sup> Physics Department, Federal University of Viçosa, Viçosa 36570-900, Brazil; eduardo.araujo@ufv.br

\* Correspondence: silvamj2003@ufv.br; Tel.: +55-31-3612-6638

**Abstract:** In this work, vanadium-substituted cesium phosphomolybdate salts with general formulae  $Cs_{3+n}PMo_{12-n}V_nO_{40}$  ( $n = 0, 1, 2,$  and  $3$ ) were synthesized and evaluated in the acetalization of benzaldehyde with alkyl alcohols. All the catalysts were characterized through Raman, infrared, and ultraviolet–visible spectroscopies, powder X-ray diffraction patterns, isotherms of  $N_2$  desorption/adsorption, and measurements of acidity strength. The catalytic activity of cesium phosphomolybdo vanadate salts was evaluated in the acetalization reactions of benzaldehyde with alkyl alcohols. Among the salts tested, the  $Cs_4PMo_{11}V_1O_{40}$  was the most active and selective catalyst in the conversion of benzaldehyde to methyl benzyl acetal and benzoic acid, which was obtained without the use of an oxidant agent. The impact of the main reaction parameters on the conversion and selectivity was evaluated by varying the content of vanadium per heteropolyanion, catalyst load, temperature, and alkyl alcohols. The greatest activity of the  $Cs_4PMo_{11}V_1O_{40}$  salt was assigned to the highest Brønsted acidity strength, as demonstrated by the acidity measurements and analysis of their surface properties. This solid catalyst has advantages over traditional liquid homogenous catalysts, such as low corrosiveness, a minimum generation of residues and effluents, and easy recovery/reuse. In addition, its synthesis route is easier and quicker than solid-supported catalysts and comprises a potential alternative route to synthesize acetals.

**Keywords:** cesium phosphomolybdo vanadate salts; acetalization; Keggin heteropolyacids; benzaldehyde



**Citation:** da Silva, M.J.; Ribeiro, C.J.A.; de Araújo, E.N.; Torteloti, I.M. Acetalization of Alkyl Alcohols with Benzaldehyde over Cesium Phosphomolybdo vanadate Salts.

*Processes* **2023**, *11*, 2220.

<https://doi.org/10.3390/pr11072220>

Academic Editor: Zahra Gholami

Received: 20 June 2023

Revised: 18 July 2023

Accepted: 21 July 2023

Published: 24 July 2023



**Copyright:** © 2023 by the authors. Licensee MDPI, Basel, Switzerland. This article is an open access article distributed under the terms and conditions of the Creative Commons Attribution (CC BY) license (<https://creativecommons.org/licenses/by/4.0/>).

## 1. Introduction

Acetalization reactions are an excellent route to protect carbonyl groups, a necessary step in various organic syntheses [1]. In addition, acetals are products of industrial interest and are used as an ingredient in paints, solvents, and drugs [2]. Recently, because of the growing surplus of glycerol, a co-product of biodiesel, benzaldehyde has also been used to produce bio-additives [3,4].

Traditionally, acetals have been obtained through Brønsted acid-catalyzed reactions (i.e.,  $H_2SO_4$  or  $HCl$ ) [5]. However, the main drawbacks of this synthesis route are high corrosiveness, the large generation of effluents, and neutralization residues in the purification steps [5–7].

As an alternative, several heterogeneous acid catalysts have been used in these processes, such as resin sulfonic, metal oxides, carbon materials, ionic liquids, zeolites, and mainly solid-supported acid dopants, which are generally matrixes with a high surface area, such as mesoporous silica [1,8–14]. Despite their undeniable success, most of the solid-supported catalysts require a laborious multistep synthesis, including the preparation of support, steps of anchoring of active phases, and thermal treatment.

In this sense, Keggin heteropolyacids (HPAs) have been proposed as a potential option because can they be used as solid salt catalysts; they are more easily synthesized, and

they avoid the drawbacks of solid-supported catalysts, such as leaching problems and deactivation [15].

Keggin HPAs are clusters of metal–oxygen composed of twelve octahedra units ( $\text{MO}_6$ ;  $\text{M} = \text{Mo}, \text{W}$ ) sharing vertices and corners, surrounding an  $\text{XO}_4$  unit in tetrahedral coordination, where X is a heteroatom ( $\text{X} = \text{P}^{5+}, \text{Si}^{4+}$ ) [16]. The arrangement of heteropolyanions (the primary structure) with hydration water molecules, di-hydronium cations, and/or transition metal cations gives the secondary structure, in which a tri-dimensional packing generates the solid particles [17].

Keggin HPAs, such as the  $\text{H}_3\text{PMo}_{12}\text{O}_{40}$ , can be converted to salts through different routes: (i) exchanging the protons with  $\text{M}^{\text{X}+}$  cations (i.e.,  $\text{M}_{3/\text{x}}\text{PMo}_{12}\text{O}_{40}$ ) [18]; (ii) hydrolyzing the  $\text{H}_3\text{PMo}_{12}\text{O}_{40}$  acid at  $\text{pH} = 4.5$  with  $\text{NaHCO}_3$ , which results in the removal of one MoO unit and provides a lacunar salt (i.e.,  $\text{Na}_7\text{PMo}_{11}\text{O}_{39}$ ) [19]; (iii) filling the vacancy of lacunar salt with an  $\text{M}^{\text{X}+}$  metal cation, giving a metal-substituted salt (i.e.,  $\text{Na}_{7-\text{x}}\text{PMo}_{11}\text{MO}_{39}$ ) [20]; and (iv) replacing “n”  $\text{Mo}^{6+}$  cations with “n”  $\text{V}^{5+}$  ions, generating an acid with the general formula  $\text{H}_{3+\text{n}}\text{PMo}_{12-\text{n}}\text{V}_\text{n}\text{O}_{40}$ , which can be converted to any one of the salts previously cited (i.e.,  $\text{M}_{3+\text{n}}\text{Pmo}_{12-\text{n}}\text{V}_\text{n}\text{O}_{40}$ ,  $\text{Na}_{7+\text{n}}\text{PMo}_{11-\text{n}}\text{V}_\text{n}\text{O}_{39}$ , or  $\text{Na}_{7+\text{n}-\text{x}}\text{PMo}_{11+\text{n}}\text{MV}_\text{n}\text{O}_{39}$ ) [21]. Therefore, due to their bi-functional acidity (i.e., Lewis and Brønsted acidity), vanadium-substituted phosphomolybdate catalysts are potential candidates to be effective catalysts in acetalization reactions.

It is important to note that the size of the ionic radius of the  $\text{M}^+$  cation is a key aspect that will determine important properties of the salts, such as surface area, porosity, and solubility; only salts containing cations with an ionic radius greater than 1.3 Å will give insoluble salts in polar solvents [22]. When small cations, such as  $\text{Fe}^{3+}$  or  $\text{Ni}^{2+}$ , were used, the catalysts were active, albeit in a homogenous phase [23]. Among the different metal salts, the Cs-exchanged salts have been widely used, since the cesium heteropoly salts have a higher surface area and are mesoporous, key characteristics in heterogeneous catalysis [24]. In addition, an increase in the  $\text{Cs}^+$  substitution level in the  $\text{Cs}_\text{x}\text{H}_{3-\text{x}}\text{PW}_{12}\text{O}_{40}$  could lead to an increase in the hydrophobicity of the HPA salts [25].

Depending on the type of metal cation, these salts have been active catalysts in oxidation and/or acid-catalyzed reactions, such as dehydration, esterification, etherification, and hydrolysis [26–30]. In particular, Keggin HPAs were efficient catalysts in ketalization (i.e., involving ketones) or acetalization (i.e., with aldehydes) reactions, either with alkyl or aromatic alcohols or polyols (i.e., glycerol) [31–35]. In previous works, the performance of vanadium phosphomolybdic acid or its sodium salts was assessed in terpenic alcohol oxidation and benzaldehyde oxidative esterification reactions [34,35]. Recently, vanadium-substituted phosphomolybdic acids were also effective catalysts in oxidative esterification reactions of benzaldehyde, albeit in a homogenous phase [36].

In this work, the goal was to investigate the activity of vanadium-substituted phosphomolybdic acid cesium salts as catalysts in acetalization reactions. To accomplish this, a series of salts with general formulae  $\text{Cs}_{3+\text{n}}\text{PMo}_{12-\text{n}}\text{V}_\text{n}\text{O}_{40}$  ( $\text{n} = 0, 1, 2, \text{ and } 3$ ) was synthesized. All the prepared catalysts were characterized by Raman, infrared, ultraviolet–visible spectroscopies, powder X-ray diffraction patterns, isotherms of nitrogen desorption/adsorption, and measurements of acidity strength. The impacts of the main reaction variables, such as time, temperature, catalyst load, and type of alcohol, were assessed.

## 2. Materials and Methods

### 2.1. Chemicals

All chemicals were acquired from commercial sources. Benzaldehyde and alkyl alcohols were all obtained from Sigma-Aldrich (99 wt.%). Hydrate  $\text{H}_3\text{PMo}_{12}\text{O}_{40}$  (99 wt.%) and the other synthesis precursors,  $\text{V}_2\text{O}_5$  (99.6 wt.%),  $\text{MoO}_3$  (99.5 wt.%),  $\text{H}_3\text{PO}_4$  (85 wt.%),  $\text{NaVO}_3$  (98 wt.%), and  $\text{Na}_2\text{MoO}_4$  ( $\geq 98$  wt.%), were also obtained from Sigma-Aldrich (St. Louis, MO, USA).

### 2.2. Synthesis of the $Cs_3PmO_{12}O_{40}$ Acid

The  $Cs_3PmO_{12}O_{40}$  acid was prepared from the precursor  $H_3PmO_{12}O_{40}$ . This was synthesized according to the literature [28,37]. The solid  $H_3PmO_{12}O_{40}$  (4.20 g) was dissolved in an aqueous solution (60 mL). To this solution was slowly added another one (40 mL) containing dissolved CsCl (1.14 g). This mixture was heated at 363 K and stirred for 3 h, resulting in the precipitation of a green solid  $Cs_3PmO_{11}O_{40}$ . After water vaporization at 373 K, the solid was collected and dried in an oven at 393 K for 24 h.

### 2.3. Synthesis of the $Cs_4PmO_{11}VO_{40}$ Salt

The  $Cs_4PmO_{11}VO_{40}$  salt was prepared from the  $H_4PmO_{11}VO_{40}$  according to the literature [35–37]. Typically, an aqueous solution CsCl (20 mL, 1.46 g) was gently added to another solution containing  $H_4PmO_{11}VO_{40}$  (60 mL, 3.86 g), leading to the formation of a yellow solid ( $Cs_4PmO_{11}VO_{40}$ ). The resulting suspension was stirred for 3 h and heated to 363 K. After water vaporization at 373 K, the solid  $Cs_4PmO_{11}VO_{40}$  salt was collected and dried in an oven at 393 K for 24 h.

### 2.4. Synthesis of the $Cs_5PmO_{10}V_2O_{40}$ Salt

The  $Cs_5PmO_{10}V_2O_{40}$  salt was prepared from the  $H_5PmO_{10}V_2O_{40}$ , which was synthesized according to the original [37] and adapted procedures [28,38]. An aqueous solution containing CsCl (20 mL, 1.76 g) was gently added to a solution of  $H_5PmO_{10}V_2O_{40}$  (60 mL, 3.62 g), producing a brown precipitate ( $Cs_5PmO_{10}V_2O_{40}$ ). The suspension was stirred for 3 h and heated to 363 K. Afterwards, the water was vaporized (373 K), and the solid dried in an oven at 393 K for 24 h.

### 2.5. Synthesis of the $Cs_6PmO_9V_3O_{40}$ Salt

To synthesize the  $Cs_6PmO_9V_3O_{40}$  salt, a similar procedure was performed, but with an adjustment to the stoichiometry of the reactants [28,38,39]. An aqueous solution containing dissolved CsCl (20 mL, 2.04 g) was slowly added to a solution of  $H_6PmO_9V_3O_{40}$  acid (60 mL, 3.40 g), resulting in a white precipitated ( $Cs_6PmO_9V_3O_{40}$ ). Then, the solution was stirred and heated at 363 K/3 h. After water vaporization, the solid was dried in an oven at 393 K for 24 h.

### 2.6. Catalysts Characterization

In the supplemental materials is a visual comparison of phosphomolybdate salts with different vanadium loads (Figure S1) and these salts with their respective precursor acids (Figure S2).

The catalyst salts were characterized through analyses of powder XRD patterns collected at angles  $2\theta$  varying from 5 to 80 degrees, using an XRD X-ray Diffraction System model D8-Discover Bruker with Ni-filtered Cu- $\alpha$  radiation ( $\lambda = 1.5418 \text{ \AA}$ ) operating at 40 kV and 40 mA. The infrared spectra of cesium phosphomolybdate salts were recorded on the Varian 660-IR spectrometer 660-IR model with FT-IR/ATR. Their UV-Vis spectra were obtained using AJX-6100 PC Micronal equipment of double beam, equipped with tungsten and deuterium lamps to provide visible (glass cuvette) and ultraviolet wavelengths (quartz cuvette), respectively. Raman spectra were recorded in the range of 100–1300  $\text{cm}^{-1}$  on a Renishaw in a Raman spectrometer working with a laser with a 633 nm wavelength.

The thermal stability and the hydration water numbers of undoped and vanadium-doped phosphomolybdic acid cesium salts were estimated by thermogravimetric analysis on a TGA/DSC-6000 Perkin-Elmer (Waltham, MA, USA) thermobalance up to 973 K. The textural properties of these salts were studied by  $N_2$  desorption/adsorption at 77 K using NOVA 1200e High Speed, Automated Surface Area, and Pore Size Analyzer Quantachrome Instruments (Boynton Beach, FL, USA). The pore size distribution calculations were conducted using the BJH adsorption-desorption method. The samples were previously degassed for 1 h. The surface area was calculated by Brunauer-Emmett-Teller equation applied to the desorption/adsorption isotherms.

The acidity strength of cesium salts was investigated through potentiometric titration with *n*-butylamine. The electrode potential variation was measured with a potentiometer (i.e., Bel, model W3B, glass electrode). Typically, the salt (50 mg) was dissolved in CH<sub>3</sub>CN, kept under magnetic stir for 3 h, and titrated with *n*-butylamine solution (ca. 0.025 mol L<sup>-1</sup>).

### 2.7. Identification of Main Reaction Products

The main reaction products were identified in a Shimadzu GC-2010 gas chromatograph (Shimadzu, Kyoto, Japan) coupled with a MS-QP 2010 mass spectrometer, operating at impact electronic mode (70 eV), within the *m/z* range of 50 to 450.

### 2.8. Catalytic Tests

Catalytic runs were carried out in a three-necked glass flask (approx. 25 mL), fitted with a reflux condenser and sampling septum. Benzaldehyde was the model aldehyde. Typically, benzaldehyde (2.77 mmol) was magnetically stirred and solved in CH<sub>3</sub>OH (10 mL) at 298 K. The addition of the acid catalyst (0.050 mol %) started the reaction.

The reaction progress was followed for 2 h, periodically collecting aliquots and analyzing them in GC equipment (Shimadzu 2010, FID) fitted with a Carbowax 20M capillary column (30 m length, 0.25 mm i.d., 0.25 mm film thickness). The temperature program was as follows: 80 °C (3 min), heating rate (10 °C min<sup>-1</sup>) until 240 °C. Injector and detector temperatures were 250 °C and 280 °C, respectively. Equations (1) and (2) provided the conversion of benzaldehyde and the product's selectivity.

$$\% \text{ conversion} = \frac{A_i - A_r}{A_i} \times 100 \quad (1)$$

where *A<sub>i</sub>* is the initial area of GC peak of benzaldehyde and *A<sub>r</sub>* is the remaining area of GC peak of benzaldehyde.

$$\% \text{ selectivity of benzaldehyde acetal} = \frac{A_p}{A_i - A_r} \times 100 \quad (2)$$

where *A<sub>p</sub>* is the benzaldehyde acetal GC peak-corrected area, *A<sub>i</sub>* is the initial area of GC peak of benzaldehyde, and *A<sub>r</sub>* is the remaining area of GC peak of benzaldehyde.

$$\% \text{ selectivity of benzoic acid} = \frac{A_p}{A_i - A_r} \times 100 \quad (3)$$

where *A<sub>p</sub>* is the benzoic acid GC peak-corrected area, *A<sub>i</sub>* is the initial area of GC peak of benzaldehyde, and *A<sub>r</sub>* is the remaining area of GC peak of benzaldehyde.

The difference between the consumed area of the GC peak of benzaldehyde (*A<sub>i</sub>* – *A<sub>r</sub>*) and the sum of the GC peak-corrected areas ( $\Sigma A_p$ ) provides the selectivity of the oligomers (Equation (4)).

$$\% \text{ oligomers} = \frac{\text{consumed benzaldehyde GC peak} - \text{the sum of the products GC peak-corrected areas}}{\text{consumed benzaldehyde GC peak area}} \times 100 \quad (4)$$

## 3. Results

### 3.1. Catalyst Characterization

#### 3.1.1. Measurements of Acid Site Strength

The potentiometric titration evaluates the strength of acidity according to the value of the initial electrode potential: *E<sub>i</sub>* > 100 mV denotes very strong sites, 0 < *E<sub>i</sub>* < 100 mV denotes strong sites, –100 < *E<sub>i</sub>* < 0 denotes weak sites, and *E<sub>i</sub>* < –100 mV denotes very weak sites [40].

Aiming for a better evaluation of the vanadium load impact on the acidity strength of vanadium-doped phosphomolybdic salts will be useful to understand what happens when the same procedure is carried out on the precursor acids.

Previously, Serwicka et al. carried out TPD–pyridine analyses of a series of  $H_{3+n}PMo_{12-n}V_nO_{40}$  ( $n = 0, 1, 2,$  or  $3$ ) acids and concluded that a load greater than a 1:11 (V:Mo) proportion increased the acidity strength [41]. This replacement modified the charge on the terminal oxygen atoms, increasing the acidity of the new proton. Vilabrille et al. ascribed this effect to the exchanges of  $Mo^{6+}$  with  $V^{5+}$  into a Keggin anion, which weakened the P–O<sub>a</sub> bond and its interaction with the di- $H_5O_2^+$  cations, increasing the strength of the acidity [42]. Recently, infrared spectra obtained from unsubstituted and vanadium-substituted phosphomolybdic acids demonstrated this effect [35,36]. On the other hand, the increase in the negative charge in the heteropolyanion triggered by a higher vanadium load (i.e.,  $PMo_{12}O_{40}^{3-}$ ,  $PMo_{11}VO_{40}^{4-}$ ,  $PMo_{10}V_2O_{40}^{5-}$ , and  $PMo_9V_3O_{40}^{6-}$ ) caused the interaction with the protons to become stronger; for this reason, di- and tri-substituted anion acids had a lower acidity strength [38]. When acids with 2:10 or 3:9 (V: Mo proportions) were prepared, the number of acid sites and their acidity strength diminished [41]. In that work, the sequence of acidity strength was  $H_4PMo_{11}VO_{40} > H_3PMo_{12}O_{40} > H_5PMo_{10}V_2O_{40} \gg H_6PMo_9V_3O_{40}$  [32]. Moreover, all the acid catalysts were classified as very strong ( $E_i > 100$  mV), except the  $H_6PMo_9V_3O_{40}$ , which presented weak acid sites ( $-100$  mV  $< E_i < 0$  mV) [36].

Notwithstanding, herein we have synthesized vanadium-substituted cesium salts, which hypothetically should have had no protons. However, a residual number of protons was sometimes detected due to the hydrolysis that the metal cation underwent, which generated  $H_3O^+$  cations [43]. Their potentiometric titration curves are presented in Figure 1.

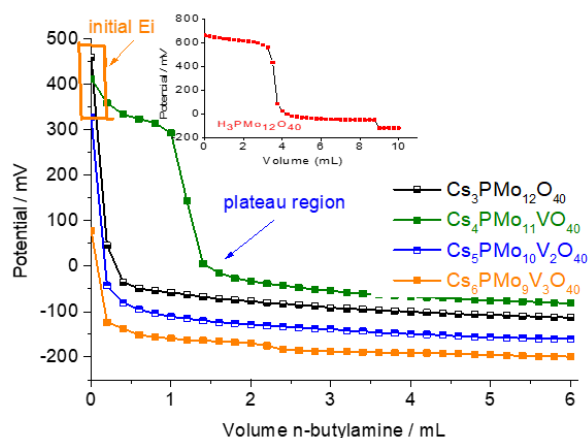


**Figure 1.** Potentiometric titration curves with n-butylamine of the pristine phosphomolybdic acid and their vanadium-substituted cesium salts.

It is important to highlight that while the vanadium-substituted phosphomolybdic acids were soluble, the cesium salts were almost insoluble. Therefore, it is more pertinent that we discuss the strength of their acid sites, instead of the strength of that acidity. The literature suggested that an increase in the V/P proportion in the vanadium-substituted phosphomolybdic acid catalysts led to a strong decrease in the acidity [44]. The initial electrode potential suggested that the acidity strength followed the tendency  $Cs_3PMo_{12}O_{40} > Cs_4PMo_{11}VO_{40} > Cs_5PMo_{10}V_2O_{40} > Cs_6PMo_9V_3O_{40}$  (Figure 1). Expectedly, the soluble  $H_3PMo_{12}O_{40}$  was the strongest acid, and the profile of the titration curve showed evidence of a greater number of protons, as measured by the volume spent to reach the plateau region. Different from that which was observed in the literature when the vanadium-substituted phosphomolybdic acids were titrated [36], the impact of the increase in vanadium load on the acidity strength (initial electrode potential value) was not too intense. However, the same effect occurred—a greater vanadium load led to a gradual decrease in the strength of the acid sites.

The profiles of the titration curves of the solid cesium salts were also distinct. While a minimum addition of a base triggered a strong fall in the potential measured in the suspension of the unsubstituted, di-, or tri-substituted salts, for the mono-substituted salts,

it was possible to note that a greater base volume was initially consumed, suggesting a higher number of acid sites than for the other salts. Nonetheless, after reaching the first plateau, a strong fall was noticed, and a new plateau was observed after the addition of 1.5 mL of base.

Ji. et al. prepared a series of cesium-exchanged partially phosphomolybdovanadate salts and evaluated their acidity using pyridine infrared spectroscopy [45]. Those authors verified that the spectrum of  $H_{1.5}Cs_{2.5}PMo_{11}VO_{40}$  presented IR absorption bands at 1444, 1533, and  $1484\text{ cm}^{-1}$ , which were assigned to adsorption in acid sites of Lewis, Brønsted, or both acid sites. Hence, the results demonstrated the presence of both Lewis and Brønsted acid sites on the catalyst surfaces.

### 3.1.2. Infrared Spectroscopy

The typical absorption bands of the vibration of chemical bonds of the Keggin anion were noticed in the region as fingerprints ( $1200$  to  $400\text{ cm}^{-1}$ ). These vibrations characterized the anion that had a Keggin-type structure. For the Keggin anion  $Mo_{12}O_{40}^{3-}$ , the bands noticed at  $1073$ ,  $965$ ,  $885$ , and  $775\text{ cm}^{-1}$  were assigned to the vibration of  $\nu_{as}P-O_a$ ,  $\nu_{as}Mo-O_d$ ,  $\nu_{as}Mo-O_b-Mo$ , and  $\nu_{as}Mo-O_c-Mo$  bonds. The subscripts distinguish the oxygen atoms concerning the place occupied in the anion.

The infrared spectra of the cesium salts exhibited the characteristic bands of the Keggin anion at  $1061\text{ cm}^{-1}$   $\nu(P-O_a)$ ,  $966\text{ cm}^{-1}$   $\nu(Mo-O_d)$ ,  $865\text{ cm}^{-1}$   $\nu(Mo-O_b-Mo)$ , and  $795\text{ cm}^{-1}$   $\nu(Mo-O_c-Mo)$ , as well as  $\delta(O-P-O)$   $594\text{ cm}^{-1}$  for the bending of the central oxygen atom [46]. It was also possible to see the rise of the shoulders or peaks split at  $1076$  and  $997\text{ cm}^{-1}$  (i.e.,  $Cs_4PMo_{11}VO_{40}$ ), which were assigned to the symmetry loss triggered by the replacement of Mo with V atoms [47].

Figure 2 shows that the infrared spectra of cesium salts with 0 or 1 vanadium atoms/per anion display almost the same bands at the same wavenumber. When 2 V atoms replaced the Mo atoms in the Keggin anion, the absorption bands were shifted toward the lower wavenumber, indicating a weakness of the  $V^{5+}-O$  chemical bonds compared with the  $Mo^{6+}-O$  bonds. However, in the infrared spectrum of the  $Cs_6PMo_9V_3O_{40}$  salt, new absorption bands were raised, which were provoked by the split of the bands that were previously present, while others were shifted. The position of the bands was linked to the strength of the bonds; nonetheless, the infrared spectrum was also a reflex of the symmetry of the heteropolyanion. Therefore, if an increase in the vanadium load leads to a decrease in symmetry, it can shift and/or result in the appearance of new bands [46].

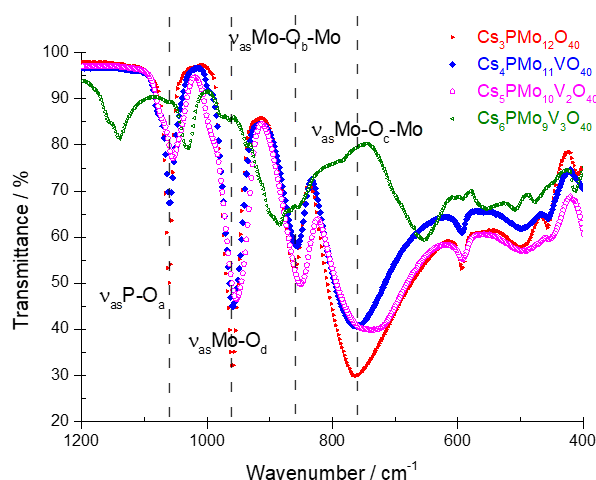


**Figure 2.** Infrared spectra of cesium salts of pristine and vanadium-substituted phosphomolybdic acids.

The literature has described that when phosphomolybdic acids were substituted with vanadium atoms, their infrared spectra were similar until 2 mol V/anion; a load of 3 mol of

V led to the shift and rise of new bands and shoulders [35,36,48]. The cesium salts of these acids underwent the same effect; when they were prepared with 0, 1, or 2 vanadium/per mol, their infrared spectra had a profile like to those of acids. Conversely, the infrared spectrum of  $\text{Cs}_6\text{PMo}_9\text{V}_3\text{O}_{40}$  also presented new bands and shoulders [34,35]. Figure 2 shows that a similar effect occurred when the phosphomolybdic acid was substituted with vanadium and converted to cesium salts.

The integrity of the Keggin anion can be assured when the infrared spectrum of the salt synthesized was equal to their precursor HPA. Therefore, the infrared data suggested that  $\text{Cs}_3\text{PMo}_{12}\text{O}_{40}$ ,  $\text{Cs}_4\text{PMo}_{12}\text{VO}_{40}$ , and  $\text{Cs}_5\text{PMo}_{10}\text{V}_2\text{O}_{40}$  had their Keggin structure preserved after the synthesis. Nonetheless, it cannot be assured for the  $\text{Cs}_6\text{PMo}_{10}\text{V}_3\text{O}_{40}$ , due to the higher loss of symmetry.

### 3.1.3. Powder XRD Patterns

While infrared spectroscopy provides information concerning the Keggin anion (primary structure), the X-ray diffractograms provide data on the secondary structure, which result from the heteropolyanion packing. The alteration of the number of hydration water molecules and/or the exchanges of  $\text{H}_3\text{O}^+$  or  $\text{H}_5\text{O}_2^+$  ions with metal cations that have different ionic radii may also impact the Keggin anion's secondary structure. Figure 3 displays the powder X-ray patterns of phosphomolybdic acid and its salts with or without vanadium.

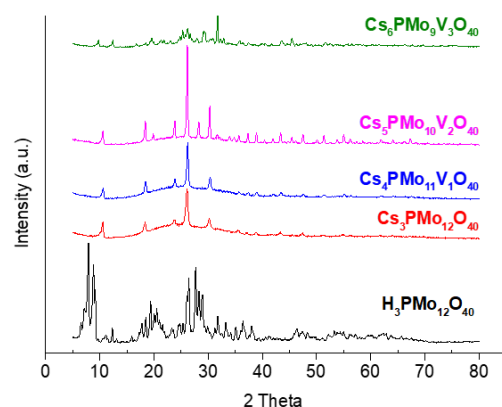


**Figure 3.** Powder XRD patterns of phosphomolybdate acid and their cesium salts with or without vanadium.

The most intense diffraction peaks of phosphomolybdic acid were also observed at  $2\theta = 8^\circ, 9^\circ, 26^\circ, 28^\circ,$  and  $29^\circ$  angles. The split of the peaks at low angles ( $2\theta = 8^\circ, 9^\circ$ ) is associated with a triclinic crystal form. However, this disappeared in the XRD diffractograms [49,50]. The diffraction patterns obtained from unsubstituted salt and those with 1 or 2 V atoms were very similar, with main peaks at  $2\theta = 10^\circ, 20^\circ, 28^\circ,$  and  $32^\circ$ . The diffraction patterns of di-substituted-vanadium cesium salt had more peaks than other salts, according to the literature [41,47]. Previously, we verified that when phosphomolybdic acids were substituted with 1, 2, or 3 vanadium mol per mol of heteropolyanion, their powder XRD patterns were retained [51].

The diffraction peaks of tri-substituted-vanadium cesium salt had a lower intensity. Regardless of their different intensities, it is possible to suppose that the XRD diffractograms of cesium heteropoly salts containing 1 or 2 vanadium did not present significant changes, even for that of  $\text{Cs}_6\text{PMo}_{10}\text{V}_3\text{O}_{40}$ . All of them had a comparable level of crystallinity, which increased with the cesium charge. The vanadium load on the phosphomolybdic acids could change their powder XRD patterns; for instance, the literature suggests a body-triclinic T crystalline structure for the  $\text{H}_4\text{PMo}_{11}\text{VO}_{40}$  and the body-centred cubic structure [44]. Comparing our data with the literature, we can conclude that the secondary structure of vanadium-mono or di-substituted cesium salts was cubic and remained almost intact after including vanadium atoms [49,50,52]. From the powder XRD pattern, it was possible

to estimate the crystal size of the cesium salts, which were calculated from the Scherrer equation (Table S1). We verified that the conversion of phosphomolybdic acid to cesium salts, as well as an increase in the vanadium load, grew the crystallite size.

#### 3.1.4. Thermal Analyses

Thermal analyses of the phosphomolybdic acid cesium salts with or without vanadium were carried out (Figures S3 and S4, see supplemental material). Regardless of the vanadium content, the thermal comportment of the phosphomolybdate salts was very similar. From these data, the number of hydration water mol was determined (Table S2), which were 3, 14, 18, and 6 water mol per heteropolyanion mol. An increase in vanadium load implied a higher cesium load, which led to a decrease in the hydration level. Possibly, the presence of large-radius cations, such as cesium in higher amounts, hampered the interaction of water with the heteropolyanion. Tan et al. studied the cesium absorption by the phosphomolybdate anions [53]. Those authors concluded that cesium ions could be easily adsorbed at the bridge oxygen sites of the four-membered rings on the surface of the  $[\text{PMo}_{12}\text{O}_{40}]^{3-}$  heteropolyanion, an aspect that we judge difficult for water interaction, leading to a lower hydration level.

The TG curves of the salts showed that after 473 K, there was a continuous decrease in the weight due to the decomposition of the heteropolyanion to oxides of phosphorous and metals present in the catalysts [39,49].

#### 3.1.5. Surface Area and Porosimetry Properties

The surface area and porosity of the cesium phosphomolybdate salts were investigated (Table S2). When the  $\text{H}_3\text{PMo}_{12}\text{O}_{40}$  acid was converted to  $\text{Cs}_3\text{PMo}_{12}\text{O}_{40}$  salt, its surface jumped from 3.8 to 104.1  $\text{m}^2\text{g}^{-1}$ , while the pore volume increased from 1.7 to 37.3  $\text{cm}^3\text{g}^{-1}$  (Table S2). It is known that the replacement of  $\text{H}^+$  ions with large-radius cations, such as  $\text{Cs}^+$ , strongly impacts its tertiary structure, creating micro- and/or mesopores and, consequently, increasing its surface area [49–54].

The literature has described that the surface area of acids, such as  $\text{H}_3\text{PW}_{10}\text{Mo}_2\text{O}_{40}$  and their cesium salts, were enhanced following the sequence  $\text{H}_3\text{PW}_{10}\text{Mo}_2\text{O}_{40} < \text{CsH}_2\text{PW}_{10}\text{Mo}_2\text{O}_{40} < \text{Cs}_2\text{HPW}_{10}\text{Mo}_2\text{O}_{40} < \text{Cs}_3\text{PW}_{10}\text{Mo}_2\text{O}_{40}$ , according to the increase in Cs loading [45]. Notwithstanding, herein an increase in vanadium load gradually diminished the surface area, which was 55.6, 4.5, and 2.8  $\text{m}^2\text{g}^{-1}$ , for the mono-, di-, and tri-vanadium phosphomolybdate cesium salts, respectively (Table S2). These results show that the surface area decreased with an increase in the V/P molar ratio of the catalysts. Possibly, this happened due to a bulk crystallite formation [44]. Indeed, the XRD patterns in Figure 3 show that these catalysts appeared to be more crystalline.

The nitrogen adsorption–desorption isotherms of all phosphomolybdic acid cesium salts were studied (Figure S5), which showed a quick initial increase corresponding to the formation of the first layer; afterward, an increase in pressure formed the second layer of the adsorbed molecules, followed by another layer (Figure S5). All the salts exhibited type IV isotherms with an H-4 hysteresis loop. The presence of the hysteresis cycle in all the isotherms demonstrated the irreversibility of the nitrogen adsorption–desorption steps.

An increase in the vanadium load reduced the pore volume of the salts; nonetheless, the distribution profile of the pore diameter of unsubstituted salt was similar to the vanadium in the other salts (Figure S5).

#### 3.1.6. Raman Spectroscopy

To analyze the effect of the vanadium substitution on the structure of the phosphomolybdic acid cesium salt catalysts, Raman spectroscopy analyses were recorded, and the spectra are shown in Figure 4.

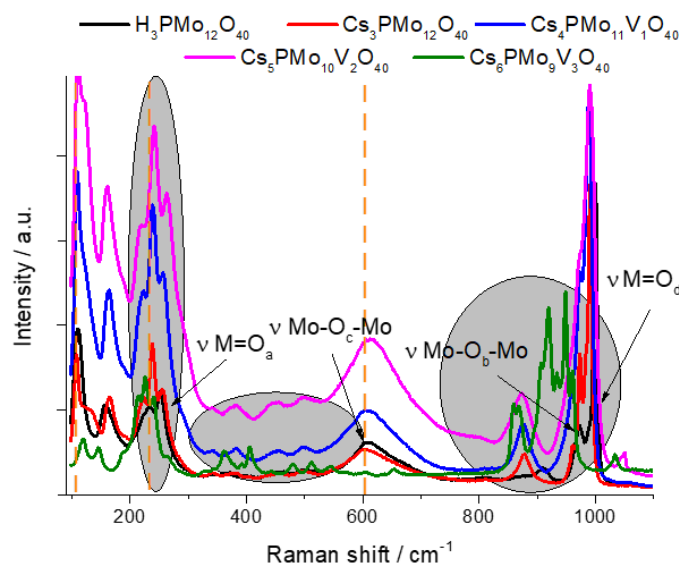


**Figure 4.** Raman spectra of unsubstituted and vanadium-substituted phosphomolybdic acid cesium salts.

An intense scattering band typical of a phosphomolybdate anion was noticed in the Raman spectra at  $1011\text{ cm}^{-1}$ , which was assigned to the symmetrical stretching of the  $W=O_d$  bond (i.e., terminal oxygen bond), present in both the acids and their heteropoly salts [55]. In the Raman spectrum of the pristine acid, this band presented only a shoulder, attributed to the  $\nu(\text{Mo}-O_b-\text{Mo})$  bond [56]. Concerning the pristine acid, this band was shifted in the cesium salt Raman spectrum, due to the modification of the intermolecular anion–anion interactions, which changed the charge density. The other scattering bands at  $849$ ,  $817$ ,  $656$ , and  $286\text{ cm}^{-1}$  wavenumbers could be assigned to the  $\text{Mo}=O_d$ ,  $\text{Mo}-O_b-\text{Mo}$ ,  $\text{Mo}-O_c-\text{Mo}$ , and  $\text{Mo}-O_a$  bonds, respectively [57].

The difference between the  $\text{Cs}^+$  and  $\text{H}^+$  radii modified the geometry of the secondary structure, consequently altering the position of the Keggin anions. The significant shift in the typical Keggin anion Raman bands toward the wavenumber's higher region with an increase in the V/P mole ratio suggested that vanadium was incorporated into the PMA catalysts [44].

When cesium cations replaced the protons, a new band rose at  $880\text{ cm}^{-1}$ . If the doping with vanadium were to increase, a higher load of cesium would be required to achieve the charge balance; consequently, the intensity of this band would also increase. Nonetheless, new scattering bands appeared between  $850$  and  $1000\text{ cm}^{-1}$ , likely due to the presence of vanadium.

Two other important modifications can be seen when cesium and/or vanadium are included in the Keggin phosphomolybdate anion. In the region between  $350$  and  $550\text{ cm}^{-1}$ , no bands were noticed in the Raman spectra of  $\text{H}_3\text{PMo}_{12}\text{O}_{40}$  or its acid  $\text{Cs}_3\text{PMo}_{12}\text{O}_{40}$ . Conversely, all three vanadium-substituted salts presented bands in this region. This suggests that vanadium was likely responsible for these scattering bands.

Another remarkable change noticed is that while the  $\text{H}_3\text{PMo}_{12}\text{O}_{40}$  acid spectrum had a duplet band at  $250\text{ cm}^{-1}$ , in the Raman spectra of the unsubstituted or substituted-cesium salts, this band became a triplet. Moreover, the intensity of these bands increased when the vanadium and cesium load also increased. The preservation of the four typical bands of Keggin anion on the Raman spectra synthesized salts suggests that their structure was maintained [26,58,59]. Therefore, we conclude that the primary structure of the Keggin anion was maintained after the proton exchange. However, its secondary structure was undoubtedly changed when vanadium and/or cesium cations were included in the Keggin anion.

### 3.1.7. Ultraviolet–Visible Spectroscopy

The electronic properties of the Keggin HPA salts are also important to explain their catalytic performance. Figure 5 displays the UV-Vis spectra of unsubstituted or vanadium-substituted phosphomolybdic acid cesium salts, which provides information about the electronic transitions that can take place in the anion. Commonly, insoluble or partially soluble HPA salts were cloudy and produced absorbance throughout the visible portion of the spectrum due to light scattering [56]. Therefore, it is important to highlight that due to the low solubility of cesium salt, the measurements were recorded in a diluted aqueous solution ( $5 \times 10^{-6} \text{ mol L}^{-1}$ ).

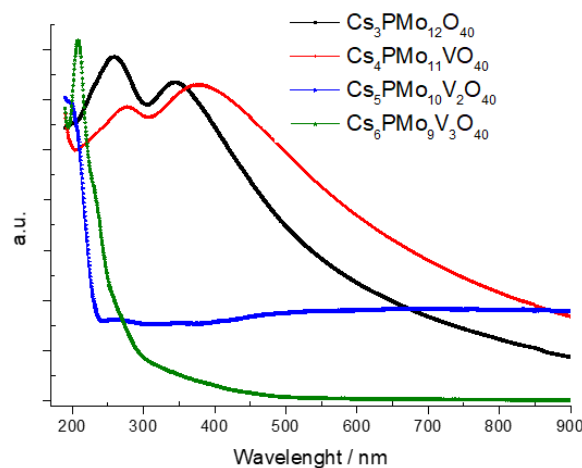


**Figure 5.** UV-Vis spectra of unsubstituted and vanadium-substituted phosphomolybdic acid cesium salts. Measurements in aqueous solutions ( $5 \times 10^{-6} \text{ mol L}^{-1}$ ).

The addenda atoms of the phosphomolybdate salts have empty “d” orbitals (i.e.,  $\text{Mo}^{6+}$ ,  $\text{V}^{5+}$ ). Therefore, the most important electronic transitions are ligand-to-metal charge transfer (i.e., LMCT). The literature describes that the UV spectrum of  $\text{H}_3\text{PMo}_{12}\text{O}_{40}$  displays two bands with maximum absorption at 220 and 320 nm, ascribed to the ligand-to-metal charge transfer transitions (LMCT) of terminal oxygen to the  $\text{Mo}^{6+}$  cation [57]. In the  $\text{Cs}_3\text{PMo}_{12}\text{O}_{40}$  sample, the LMCT bands of  $\text{Mo}^{6+}$  to  $\text{O}^{2-}$  (in octahedral coordination) were observed with an absorption maximum at 270 and 370 nm (Figure 5).

The substitution with one vanadium mol per anion mol shifted these bands to the red region, with an absorption maximum at wavelengths 280 and 390 nm. The presence of 2 or 3 vanadium mols per anion mol practically extinguished the second band. Nonetheless, the band at 280 nm was shifted to a lower wavelength. This suggests that a vanadium load of 2 or 3 mol/heteropolyanion stabilized the LUMO (low-molecular orbital unoccupied), causing the energy involved in the LMCT transition to be higher.

## 3.2. Catalytic Tests

### 3.2.1. Effect of Vanadium Load on the Phosphomolybdic Acid Salt-Catalyzed Acetalization of Benzaldehyde

The catalytic activity of phosphomolybdic acids with or without vanadium was evaluated following the conditions previously reported in the literature [36]. The kinetic curves, conversions, and reaction selectivities are shown in Figure 6.

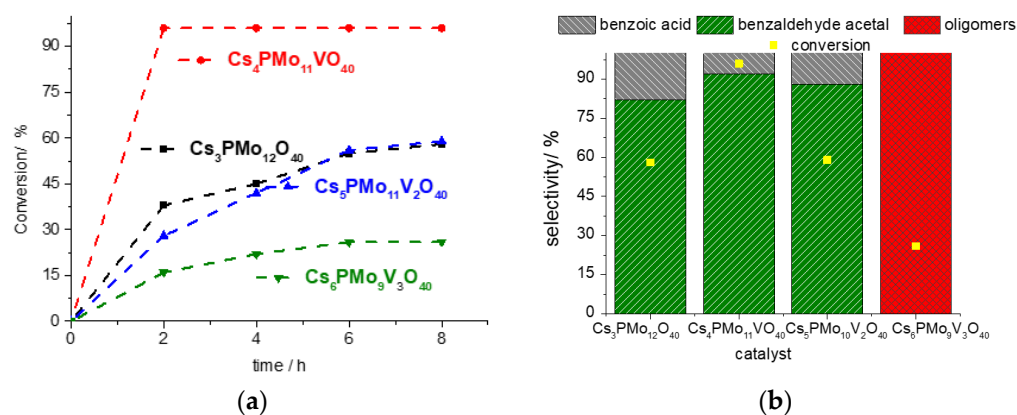
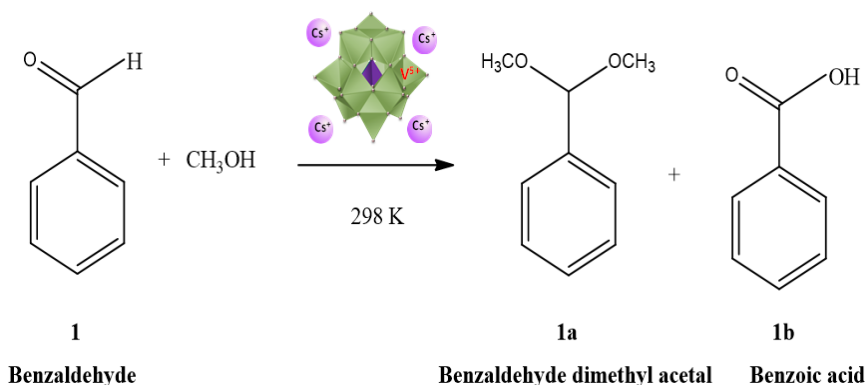


**Figure 6.** Effect of vanadium load on the activity of phosphomolybdic acid catalysts on the kinetic curves (a), conversion and selectivity after 8 h (b) of acetalization reactions of methyl alcohol with benzaldehyde. Reaction conditions: benzaldehyde (2.77 mmol), toluene (internal standard), catalyst (0.050 mol % of catalyst), temperature (298 K),  $\text{CH}_3\text{OH}$  (10 mL).

The activity of the catalysts followed the trends  $\text{Cs}_6\text{PMo}_9\text{V}_3\text{O}_{40} < \text{Cs}_5\text{PMo}_{10}\text{V}_2\text{O}_{40} \approx \text{Cs}_3\text{PMo}_{12}\text{O}_{40} \ll \text{Cs}_4\text{PMo}_{11}\text{V}_1\text{O}_{40}$  (Figure 6a). In addition to reaching the highest conversion, this salt was the most selective catalyst toward acetal formation (Figure 6b).

The acetalization process is typically an acid-catalyzed reaction. Therefore, it is hoped that most acidic catalysts will be the most efficient. Indeed, the acid sites of both the  $\text{Cs}_3\text{PMo}_{12}\text{O}_{40}$  and  $\text{Cs}_4\text{PMo}_{11}\text{V}_1\text{O}_{40}$  catalysts were the strongest, having an equal strength of acidity, as demonstrated by the  $E_i$  values in Figure 1. However, the  $\text{Cs}_4\text{PMo}_{11}\text{V}_1\text{O}_{40}$  salt demonstrated that it had the highest acid site number, as suggested by the profile of the titration curve. Even in the absence of vanadium, the  $\text{Cs}_3\text{PMo}_{12}\text{O}_{40}$  salt was more active than the two vanadium-doped catalysts, possibly due to the combination of its strong acidity with the highest surface area (Table S2).

Conversely, the poorest conversion (5%) was achieved in the  $\text{Cs}_6\text{PMo}_9\text{V}_3\text{O}_{40}$ -catalyzed reaction, which can be attributed to the lowest strength of acidity and surface area (Figure 1, Table S2). Moreover, its reaction provided only oligomers as products (Figure 6b). The reactions with all other vanadium-substituted cesium phosphomolybdates always gave acetal and benzoic acid as the main and secondary products, respectively (Scheme 1). The most acidic and efficient catalyst was also the most selective to acetal benzaldehyde.



**Scheme 1.** Main products of benzaldehyde acetalization with methyl alcohol.

Once the reactions were carried out under normal room conditions, the benzoic acid formation may have occurred due to the presence of molecular oxygen. The literature has described that vanadium-substituted phosphomolybdic acids were effective catalysts in aerobic oxidation reactions of aromatic compounds [60].

### 3.2.2. Impacts of $\text{Cs}_4\text{PMo}_{11}\text{VO}_{40}$ Load on the Benzaldehyde Acetalization

Although the catalyst concentration did not affect the equilibrium conversion, this effect was assessed to evaluate how this parameter affected the reactions of benzaldehyde with methyl alcohol within the reaction time studied. Figure 7 shows the kinetic curves (Figure 7a) and the conversion and selectivity (Figure 7b) that was achieved after 2 h in the reactions as the catalyst load varied from 0.010 to 0.050 mol %.

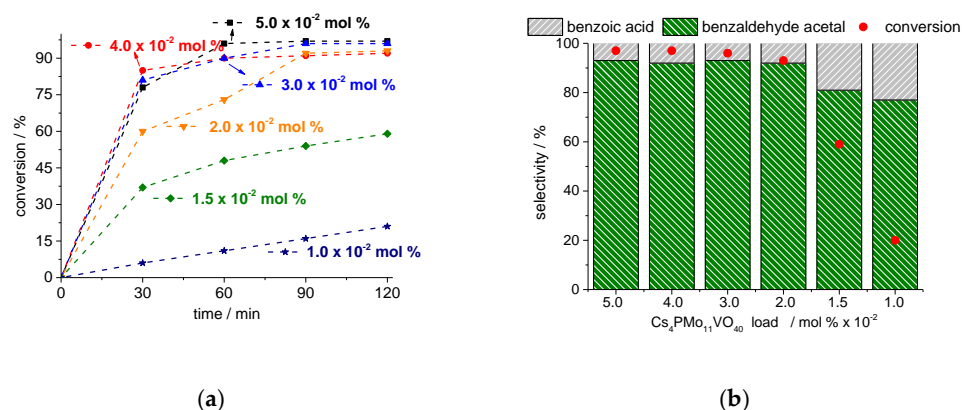


**Figure 7.** Effect of  $\text{Cs}_4\text{PMo}_{11}\text{VO}_{40}$  catalyst load on the kinetic curves (a), conversion and product selectivity (b) of benzaldehyde acetalization reactions with  $\text{CH}_3\text{OH}$  after 2 h of reaction. Reaction conditions: benzaldehyde (2.77 mmol), toluene (internal standard), catalyst (variable), temperature (298 K),  $\text{CH}_3\text{OH}$  (10 mL).

An increase in catalyst load enhanced the initial rate of reactions, causing faster reactions. This can be attributed to the higher presence of acid sites when a higher catalyst load was used. Nonetheless, after 2 h of reaction, the conversion and selectivity attained in the reactions as the load varied from 0.050 to 0.020 mol % were almost the same. Only the reactions with lower loads (i.e., 0.015 or 0.010 mol %) achieved lower conversion values.

Even when the lowest catalyst load was used, benzaldehyde acetal and benzoic acid were the reaction products formed. The variation of conversion and selectivity during the reaction was also investigated (Figure 8).

Although the reactions from 0.020 to 0.050 mol % were very similar, without significant differences in conversions or selectivity after 2 h of reaction, it is possible to verify that when the reaction was in its initial period, the benzoic acid selectivity had its maximum; afterward, it gradually diminished, consequently increasing the acetal selectivity. This was more noticeable for the lower catalyst loads. It is noteworthy that herein there were two competitive reactions; acetalization of benzaldehyde, which is more favorable when a greater number of acid sites is feasible (i.e., a high catalyst load), and oxidation, which is promoted by the vanadium-substituted catalysts [61].

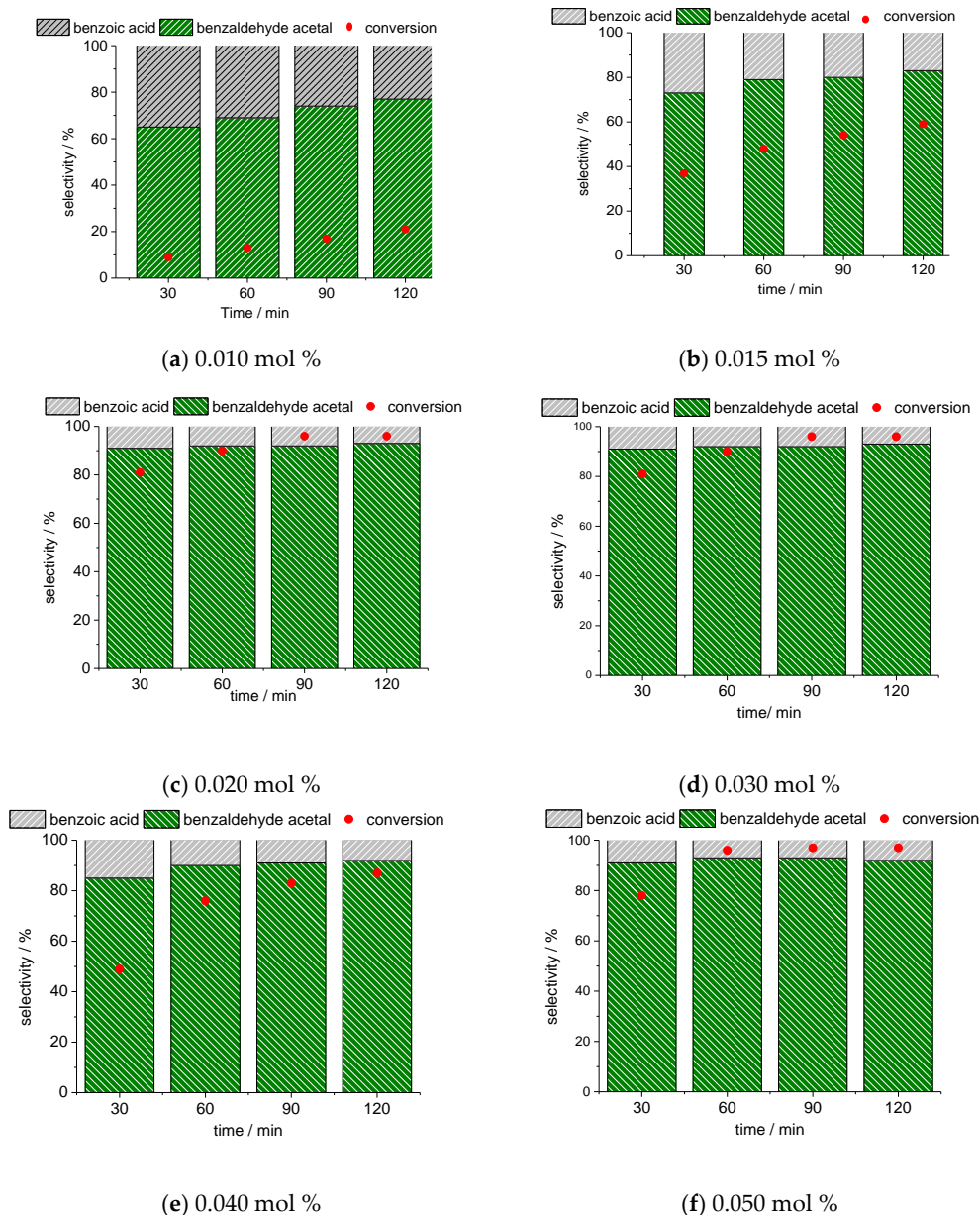


**Figure 8.** Influence of time on the conversion and selectivity of benzaldehyde acetalization reactions with  $\text{CH}_3\text{OH}$  using different loads of  $\text{Cs}_4\text{PMo}_{11}\text{VO}_{40}$  catalyst. Reaction conditions: benzaldehyde (2.77 mmol), toluene (internal standard), catalyst (variable), temperature (298 K),  $\text{CH}_3\text{OH}$  (10 mL).

### 3.2.3. Effects of Temperature on the $\text{Cs}_4\text{PMo}_{11}\text{VO}_{40}$ -Catalyzed Benzaldehyde Acetalization

When the reaction temperature increases, it is hoped that its initial rate increases, due to the higher number of effective collisions. However, undesirable reactions, such as oligomerization can be also favored, decreasing the selectivity toward the goal products. This effect was assessed, and the main results are described in Figure 9. The reactions were carried out with a lower catalyst load (0.015 mol %), aiming to highlight this effect.

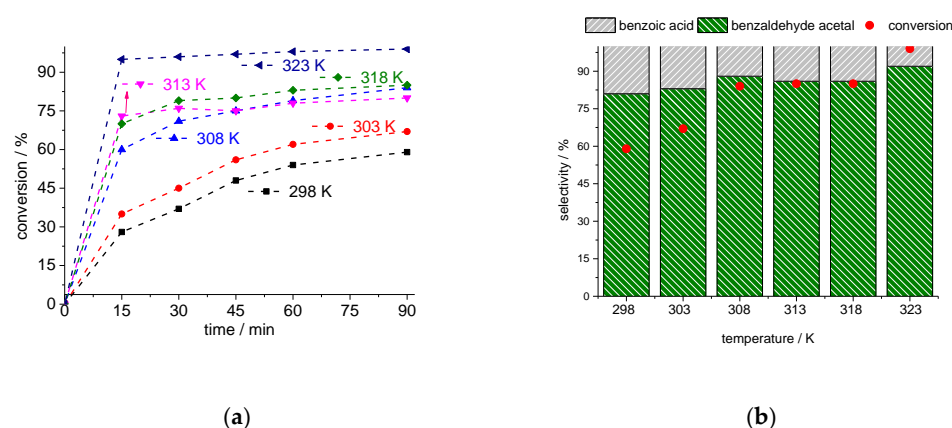


**Figure 9.** Impacts of temperature on the kinetic curves (a), conversion and selectivity (b) of  $\text{Cs}_4\text{PMo}_{11}\text{VO}_{40}$ -catalyzed benzaldehyde acetalization reactions with  $\text{CH}_3\text{OH}$  after 90 min reaction. Reaction conditions: benzaldehyde (2.77 mmol), toluene (internal standard), catalyst (0.015 mol %),  $\text{CH}_3\text{OH}$  (10 mL).

With an increase in temperature, the reactions became faster, due to a higher number of effective collisions, an effect that was much more visible at 323 K. Consequently, the conversions were gradually increased when the reactions were carried out at higher temperatures. However, within the temperature interval of 298 to 318 K, the selectivity was almost the same. Only at 323 K, the benzaldehyde acetal selectivity was increased. Moreover, regardless of temperature, no oligomer was formed.

### 3.2.4. Impacts of Alcohol on the $\text{Cs}_4\text{PMo}_{11}\text{VO}_{40}$ -Catalyzed Benzaldehyde Acetalization

The steric hindrance as well as the size of the carbon chain can affect the alcohol reactivity in acetalization reactions. This effect was investigated by carrying out reactions with different alcohols, and the main results are shown in Figure 10.

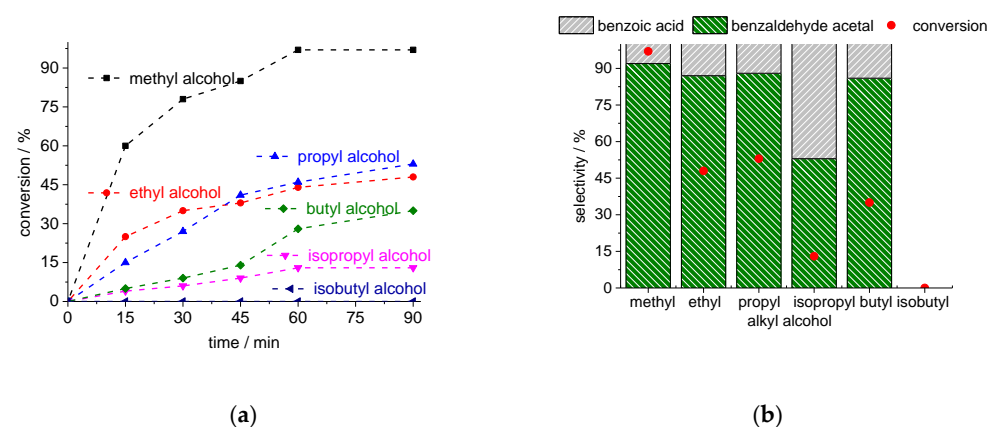
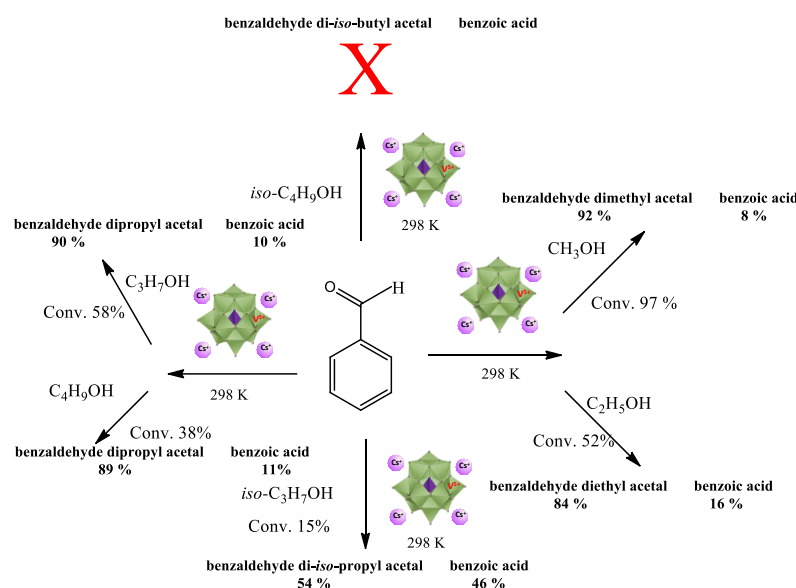


**Figure 10.** Effect of alcohol on the kinetic curves (a), conversion and selectivity after 90 min (b) of  $\text{Cs}_4\text{PMo}_{11}\text{VO}_{40}$ -catalyzed benzaldehyde acetalization reactions. Reaction conditions: benzaldehyde (2.77 mmol), toluene (internal standard), catalyst (0.050 mol %), reaction volume (10 mL).

Although methyl alcohol was much more reactive, ethyl and propyl alcohols had a similar reactivity. Among the alcohols evaluated, the reaction with butyl alcohol reached the lowest conversion. However, regardless of the carbon chain size, all the primary alcohols were very selective to benzaldehyde acetal. Conversely, the steric hindrance was a key aspect of the reactions with secondary alcohols. While the isopropyl acetalization achieved only 15% of conversion and a selectivity of 52%, isobutyl was not reactive (Scheme 2).



**Scheme 2.** Conversion and selectivity of  $\text{Cs}_4\text{PMo}_{11}\text{VO}_{40}$ -catalyzed benzaldehyde acetalization reactions.

#### 4. Conclusions

The acetalization reactions of benzaldehyde with alkyl alcohols were studied using vanadium-substituted phosphomolybdic acids as catalysts. Infrared, Raman, and powder XRD analyses showed that the structures of the Keggin anion (i.e., primary structure) remained intact after the vanadium substitution. However, the secondary structure of phosphomolybdate salts was impacted by the proton exchange with cesium cations, which have a greater ionic radius. The vanadium load also impacted the secondary structure of the catalysts, and it was more noticeable mainly in the XRD of the  $\text{Cs}_6\text{PMo}_9\text{V}_3\text{O}_{40}$  salt. Among the four phosphomolybdic acid cesium salts evaluated, the  $\text{Cs}_4\text{PMo}_{11}\text{VO}_{40}$  acid was the most active and selective toward benzaldehyde acetal, achieving an almost complete conversion and 95% selectivity to acetal, with benzoic acid as a secondary product. This was attributed to its high surface area and greatest strength of acidity, as demonstrated by the BET analysis and potentiometric titration, respectively. The effects of the main reaction variables were assessed in the reactions of benzaldehyde with methyl alcohol. An increase in the catalyst load or reaction temperature accelerated the reaction rate and enhanced the conversion and acetal selectivity. By expanding the reaction scope to other alkyl alcohols, we have found that while primary alcohols were efficiently acetalized, the secondary ones were almost unreactive.

**Supplementary Materials:** The following supporting information can be downloaded at <https://www.mdpi.com/article/10.3390/pr11072220/s1>, Figure S1. Unsubstituted cesium phosphomolybdate (first) and containing 1 (second), 2 (third), or 3 (fourth) vanadium atoms mol/mol of heteropolyanion. Figure S2. Comparison of unsubstituted cesium phosphomolybdate salt and acid (first) and acids or salts containing 1 (second), 2 (third), or 3 (fourth) vanadium atoms. Figure S3. DTG/TG curves of unsubstituted and vanadium-substituted cesium phosphomolybdate. Figure S4. Isotherms of nitrogen desorption/adsorption of unsubstituted and vanadium-substituted cesium phosphomolybdate salts. Figure S5. Diameter and volume of pores of unsubstituted and vanadium-substituted cesium phosphomolybdate salts. Table S1. Surface area, volume, and diameter of pores of phosphomolybdic acid and their vanadium-substituted cesium salts. Table S2. Crystallite sizes of phosphomolybdic acid and their vanadium-substituted cesium salts.

**Author Contributions:** Conceptualization, M.J.d.S.; methodology, M.J.d.S. and C.J.A.R.; software, M.J.d.S., E.N.d.A. and C.J.A.R.; investigation, M.J.d.S., C.J.A.R. and I.M.T.; resources, M.J.d.S., C.J.A.R. and I.M.T.; writing—original draft preparation, M.J.d.S. and C.J.A.R., writing—review and editing,

M.J.d.S. and C.J.A.R.; supervision, M.J.d.S. All authors have read and agreed to the published version of the manuscript.

**Funding:** This research was funded by Coordenação de Aperfeiçoamento de Pessoal de Nível Superior—Brasil (CAPES)—Finance Code 001.

**Data Availability Statement:** Not acceptable.

**Acknowledgments:** The authors are grateful to the Brazilian research agencies, FAPEMIG and CNPq, for the financial support.

**Conflicts of Interest:** The authors declare no conflict of interest.

## References

1. Dong, J.L.; Yu, L.S.H.; Xie, J.W. A simple and versatile method for the formation of acetals/ketals using trace conventional acids. *ACS Omega* **2018**, *3*, 4974–4985. [[CrossRef](#)]
2. Tsolakis, N.; Bam, W.; Srai, J.S.; Kumar, M. Renewable chemical feedstock supply network design: The case of terpenes. *J. Clean. Prod.* **2019**, *222*, 802–822. [[CrossRef](#)]
3. Wu, L.; Moteki, T.; Gokhale, A.A.; Flaherty, D.W.; Toste, F.D. Production of fuels and chemicals from biomass: Condensation reactions and beyond. *Chem* **2016**, *1*, 32–58. [[CrossRef](#)]
4. Sanchez, L.M.; Thomas, H.J.; Climent, M.J.; Romanelli, G.P.; Iborra, S. Heteropolycompounds as catalysts for biomass product transformations. *Catal. Rev.* **2016**, *58*, 497–586. [[CrossRef](#)]
5. Clark, J.H. Solid acids for green chemistry. *Acc. Chem. Res.* **2002**, *35*, 791–797. [[CrossRef](#)]
6. Li, J.; Liang, X. Magnetic solid acid catalyst for biodiesel synthesis from waste oil. *Energ. Conv. Manag.* **2017**, *141*, 126–132. [[CrossRef](#)]
7. Lotero, E.; Liu, Y.; Lopes, D.E.; Suwannakarn, K.; Bruce, D.A.; Goodwin, J.G. Synthesis of biodiesel via acid catalysis. *Ind. Eng. Chem. Res.* **2005**, *44*, 5353–5363. [[CrossRef](#)]
8. Hamada, N.; Kazahaya, K.; Shimizu, H.; Sato, T. An efficient and versatile procedure for the synthesis of acetals from aldehydes and ketones catalyzed by lithium tetrafluoroborate. *Synlett* **2004**, *6*, 1074–1076. [[CrossRef](#)]
9. Corma, A.; Garcia, H. Lewis Acids: From conventional homogeneous to green homogeneous and heterogeneous catalysis. *Chem. Rev.* **2003**, *103*, 4307–4366. [[CrossRef](#)]
10. Wegenhart, B.L.; Liu, S.; Thom, M.; Stanley, D.; Abu-Omar, M.M. Solvent-free methods for making acetals derived from glycerol and furfural and their use as a biodiesel fuel component. *ACS Catal.* **2012**, *2*, 2524–2530. [[CrossRef](#)]
11. Umbarkar, S.B.; Kotbagi, T.V.; Biradar, A.V.; Parsicha, R.; Chanale, J.; Dongare, M.K.; Mamede, A.S.; Lancelot, C.; Payen, E. Acetalization of glycerol using mesoporous MoO<sub>3</sub>/SiO<sub>2</sub> solid acid catalyst. *J. Mol. Catal. A* **2009**, *310*, 150–158. [[CrossRef](#)]
12. Liu, T.; Fu, W.; Zheng, X.; Jiang, J.; Hu, M.; Tang, T. Zeolite Nanofiber Assemblies as Acid Catalysts with High Activity for the Acetalization of Carbonyl Compounds with Alcohols. *RSC Adv.* **2014**, *4*, 18217–18221. [[CrossRef](#)]
13. Poyraz, A.S.; Kuo, C.-H.; Kim, E.; Meng, Y.; Seraji, M.S.; Suib, S.L. Tungsten-Promoted Mesoporous Group 4 (Ti, Zr, and Hf) Transition-Metal Oxides for Room-Temperature Solvent-Free Acetalization and Ketalization Reactions. *Chem. Mater.* **2014**, *26*, 2803–2813. [[CrossRef](#)]
14. Myles, L.; Gore, R.G.; Gathergood, N.; Connon, S.J. A New Generation of Aprotic Yet Brønsted Acidic Imidazolium Salts: Low Toxicity, High Recyclability and Greatly Improved Activity. *Green Chem.* **2013**, *15*, 2740–2746. [[CrossRef](#)]
15. da Silva, M.J.; Liberto, N.A. Soluble and solid supported Keggin heteropolyacids as catalysts in reactions for biodiesel production: Challenges and recent advances. *Curr. Org. Chem.* **2016**, *20*, 1263–1283. [[CrossRef](#)]
16. da Silva, M.J.; de Oliveira, C.M. Catalysis by Keggin heteropolyacid salts. *Curr. Catal.* **2018**, *7*, 26–34. [[CrossRef](#)]
17. Coronel, N.C.; da Silva, M.J. Lacunar Keggin heteropolyacid salts: Soluble, solid and solid-supported catalysts. *J. Clust. Sci.* **2018**, *29*, 195–205. [[CrossRef](#)]
18. da Silva, M.J.; Liberto, N.A.; Leles, L.C.A.; Pereira, U.A. Fe<sub>4</sub>(SiW<sub>12</sub>O<sub>40</sub>)<sub>3</sub>-catalyzed glycerol acetylation: Synthesis of bioadditives by using highly active Lewis acid catalyst. *J. Mol. Catal. A* **2019**, *422*, 69–83. [[CrossRef](#)]
19. Vilanculo, C.B.; da Silva, M.J. Unraveling the role of the lacunar Na<sub>7</sub>PW<sub>11</sub>O<sub>39</sub> catalyst in the oxidation of terpene alcohols with hydrogen peroxide at room temperature. *N. J. Chem.* **2020**, *44*, 2813–2820. [[CrossRef](#)]
20. da Silva, M.J.; Andrade, P.H.S.; Sampaio, V.F.C. Transition metal-substituted potassium silicotungstate salts as catalysts for oxidation of terpene alcohols with hydrogen peroxide. *Catal. Lett.* **2021**, *151*, 2094–2106. [[CrossRef](#)]
21. Vilanculo, C.B.; da Silva, M.J. Na<sub>4</sub>PMo<sub>11</sub>VO<sub>40</sub>-catalyzed one-pot oxidative esterification of benzaldehyde with hydrogen peroxide. *RSC Adv.* **2021**, *11*, 34979–34987. [[CrossRef](#)]
22. Diaz, J.; Pizzio, L.R.; Pecchi, G.; Campos, C.H.; Azócar, L.; Briones, R.; Romero, R.; Henríquez, A.; Gaigneaux, E.M.; Contreras, D. Tetrabutyl ammonium salts of Keggin-type vanadium-substituted phosphomolybdates and phosphotungstates for selective aerobic catalytic oxidation of benzyl alcohol. *Catalysts* **2022**, *12*, 507. [[CrossRef](#)]
23. Patel, A.; Patel, J. Nickel salt of phosphomolybdic acid as a bi-functional homogeneous recyclable catalyst for base free transformation of an aldehyde into ester. *RSC Adv.* **2020**, *10*, 22146–22155. [[CrossRef](#)]
24. Okuhara, T. Water-tolerant solid acid catalysts. *Chem. Rev.* **2002**, *102*, 3641–3666. [[CrossRef](#)] [[PubMed](#)]

25. Dias, A.S.; Lima, S.; Pillinger, M.; Valente, A.A. Acidic cesium salts of 12-tungstophosphoric acid as catalysts for the dehydration of xylose into furfural. *Carbohydr. Res.* **2006**, *341*, 2946–2953. [[CrossRef](#)]
26. Barteau, K.P.; Lyons, J.E.; Song, I.K.; Barteau, M.A. UV-visible spectroscopy as a probe of heteropolyacid redox properties: Application to liquid phase oxidations. *Top. Catal.* **2006**, *41*, 55–62. [[CrossRef](#)]
27. Da Silva, M.J.; Lopes, N.P.G.; Ferreira, S.O.; Da Silva, R.C.; Natalino, R.; Chaves, D.M.; Teixeira, M.G. Monoterpenes etherification reactions with alkyl alcohols over cesium partially exchanged Keggin heteropoly salts: Effects of the catalyst composition. *Chem. Pap.* **2021**, *75*, 153–168. [[CrossRef](#)]
28. Batalha, D.C.; Ferreira, S.O.; Da Silva, R.C.; Da Silva, M.J. Cesium-exchanged lacunar Keggin heteropolyacid salts: Efficient solid catalysts for the green oxidation of terpenic alcohols with hydrogen peroxide. *Chem. Select* **2020**, *5*, 1976–1986. [[CrossRef](#)]
29. Chaves, D.M.; Ferreira, S.O.; Chagas da Silva, R.; Natalino, R.; da Silva, M.J. Glycerol esterification over Sn(II)-exchanged Keggin heteropoly salt catalysts: Effect of thermal treatment temperature. *Energ. Fuels* **2019**, *33*, 7705–7716. [[CrossRef](#)]
30. da Silva, M.J.; Chaves, D.M.; Ferreira, S.O.; da Silva, R.C.; Filho, J.B.G.; Bruziquesi, C.G.O.; Al-Rabiah, A.A. Impacts of Sn(II) doping on the Keggin heteropolyacid-catalyzed etherification of glycerol with tert-butyl alcohol. *Chem. Eng. Sci.* **2022**, *247*, 116913. [[CrossRef](#)]
31. da Silva, M.J.; Chaves, D.M.; Julio, A.A.; Rodrigues, F.A.; Bruziques, C.G.; da Silva, M.J. Sn(II)-exchanged Keggin silicotungstic acid-catalyzed etherification of glycerol and ethylene glycol with alkyl alcohols. *Ind. Eng. Chem. Res.* **2020**, *59*, 9858–9868. [[CrossRef](#)]
32. da Silva, M.J.; Julio, A.A.; Ferreira, S.O.; da Silva, R.C.; Chaves, D.M. Tin(II) phosphotungstate heteropoly salt: An efficient solid catalyst to synthesize bioadditives ethers from glycerol. *Fuel* **2019**, *254*, 115607. [[CrossRef](#)]
33. Pinheiro, P.F.; Chaves, D.M.; da Silva, M.J. One-pot synthesis of alkyl levulinates from biomass derivative carbohydrates in tin(II) exchanged silicotungstates-catalyzed reactions. *Cellulose* **2019**, *26*, 7953–7969. [[CrossRef](#)]
34. Vilanculo, C.B.; Da Silva, M.J.; Rodrigues, A.A.; Ferreira, S.O.; Da Silva, R.C. Vanadium-doped sodium phosphomolybdate salts as catalysts in the terpene alcohols oxidation with hydrogen peroxide. *RSC Adv.* **2021**, *11*, 24072–24085. [[CrossRef](#)] [[PubMed](#)]
35. Vilanculo, C.B.; da Silva, M.J.; Torres, J.A.V. Vanadium-doped phosphomolybdic acids as catalysts for geraniol oxidation with hydrogen peroxide. *RSC Adv.* **2022**, *12*, 11796–11806. [[CrossRef](#)]
36. da Silva, M.J.; Ribeiro, C.J.A.; Vilanculo, C.B. How the content of protons and vanadium affects the activity of  $H_{3+n}PMo_{12-n}V_nO_{40}$  ( $n = 0, 1, 2$ , or  $3$ ) catalysts on the oxidative esterification of benzaldehyde with hydrogen peroxide. *Catal. Lett.* **2023**, *153*, 2045–2056. [[CrossRef](#)]
37. Tsigdinos, G.A.; Hallada, C. Molybdovanadophosphoric acids and their salts. I. Investigation of methods of preparation and characterization. *J. Inorg. Chem.* **1968**, *7*, 437–441. [[CrossRef](#)]
38. Chen, C.-Y.; Li, H.-X.; Davis, M.E. Studies on mesoporous materials: I. Synthesis and characterization of MCM-41. *Micropor. Mat.* **1993**, *2*, 17–26. [[CrossRef](#)]
39. Jing, F.; Katryniok, B.; Dumeignil, F.; Bordes-Richard, E. Catalytic selective oxidation of isobutane to methacrylic acid on supported  $(NH_4)_3HPMo_{11}VO_{40}$  catalysts. *J. Catal.* **2014**, *309*, 121–135. [[CrossRef](#)]
40. Pizzio, L.R.; Blanco, M.N. A contribution to the physicochemical characterization of nonstoichiometric salts of tungstosilicic acid. *Micropor. Mesopor. Mat.* **2007**, *103*, 40–47. [[CrossRef](#)]
41. Serwicka, E.M.; Bruckman, K.; Haber, J.; Paukshtis, E.A.; Yurchenko, E.A. Acid-base properties of  $H_{3+n}PV_nMo_{12-n}O_{40}$  heteropolyacids, pure and supported on  $K_3PMo_{12}O_{40}$ . *Appl. Catal.* **1991**, *73*, 153–163. [[CrossRef](#)]
42. Villabrille, P.; Romanelli, G.; Vázquez, P.; Cáceres, C. Vanadium-substituted Keggin heteropolycompounds as catalysts for eco-friendly liquid phase oxidation of 2,6-dimethylphenol to 2,6-dimethyl-1,4-benzoquinone. *Appl. Catal. A* **2004**, *270*, 101–111. [[CrossRef](#)]
43. da Silva, M.J.; Rodrigues, A.A.; Teixeira, M.G. Iron (III) Silicotungstate: An efficient and recyclable catalyst for converting glycerol to solketal. *Energ. Fuels* **2020**, *34*, 9664–9673. [[CrossRef](#)]
44. Viswanadham, B.; Jhansi, P.; Chary, K.V.R.; Friedrich, H.B.; Singh, S. Efficient solvent-free Knoevenagel condensation over vanadium containing heteropolyacid catalysts. *Catal. Lett.* **2016**, *146*, 364–371. [[CrossRef](#)]
45. Li, X.-K.; Zhao, J.; Ji, W.J.; Zhang, Z.-B.; Chen, Y.; Au, C.-T.; Han, S.; Hibst, H. Effect of vanadium substitution in the cesium salts of Keggin-type heteropolyacids on propane partial oxidation. *J. Catal.* **2006**, *237*, 58–66. [[CrossRef](#)]
46. Zhang, H.; Wang, T.; Ma, X.; Zhu, W. Composition, structural evolution and the related property variations in preparation of mixed cesium/ammonium acidic salts of heteropolyacids. *Catalysts* **2016**, *6*, 187. [[CrossRef](#)]
47. Rocchiccioli-Deltcheff, C.; Fournier, M. Catalysis by polyoxometalates. Part 3.-Influence of vanadium(V) on the thermal stability of 12-metaphosphoric acids from in situ infrared studies. *J. Chem. Soc. Faraday Trans.* **1991**, *87*, 3913–3920. [[CrossRef](#)]
48. Casarini, D.; Centi, G.; Jiru, P.; Lena, V.; Tvaruzkova, Z. Reactivity of molybdovanadophosphoric Acids: Influence of the presence of vanadium in the primary and secondary structure. *J. Catal.* **1993**, *142*, 325–344. [[CrossRef](#)]
49. Sun, M.; Zhang, J.; Cao, C.; Zhang, Q.; Wang, Y.; Wan, H. Significant effect of acidity on catalytic behaviours of Cs-substituted polyoxometalates for oxidative dehydrogenation of propane. *Appl. Catal. A* **2008**, *349*, 212–221. [[CrossRef](#)]
50. Khillare, K.R.; Aher, D.S.; Chavan, L.D.; Shankarwar, S.G. Cesium salt of 2-molybdo-10-tungstophosphoric acid as an efficient and reusable catalyst for the synthesis of uracil derivatives via a green route. *RSC Adv.* **2021**, *11*, 33980–33989. [[CrossRef](#)] [[PubMed](#)]
51. Sen, R.; Bera, R.; Bhattacharjee, A.; Gütlich, P.; Ghosh, S.; Mukherjee, A.K.; Koner, S. Oxo-Vanadium(IV) dihydrogen phosphate: Preparation, magnetic study, and heterogeneous catalytic epoxidation. *Langmuir* **2008**, *24*, 5970–5975. [[CrossRef](#)] [[PubMed](#)]

52. Balaraju, M.; Rekha, V.; Davi, B.L.A.P.; Prasad, R.B.N.; Prasad, P.S.S.; Lingaiah, N. Surface and structural properties of titania-supported Ru catalysts for hydrogenolysis of glycerol. *Appl. Catal. A* **2010**, *384*, 107–114. [[CrossRef](#)]
53. Tan, Z.; Dong, L.; Huang, Z.; Du, L.; Wang, X. A theoretical study on the selective adsorption of  $\text{NH}_4^+$  and  $\text{Cs}^+$  on the phosphomolybdate ion. *Colloids surf. A: Physicochem. Engin. Asp.* **2016**, *502*, 74–80. [[CrossRef](#)]
54. Okuhara, T.; Watanabe, H.; Nishimura, T.; Inumarau, K.; Misono, M. Microstructure of cesium hydrogen salts of 12-tungstophosphoric acid relevant to novel acid catalysis. *Chem. Mater.* **2000**, *12*, 2230–2238. [[CrossRef](#)]
55. Narasimharao, K.; Brown, D.R.; Lee, A.F.; Newman, A.D.; Siril, P.F.; Tavener, S.J.; Wilson, K. Structure–activity relations in Cs-doped heteropolyacid catalysts for biodiesel production. *J. Catal.* **2007**, *248*, 226–234. [[CrossRef](#)]
56. Soares, J.C.S.; Golçalves, A.H.A.; Zotin, F.M.Z.; Araújo, L.R.R.; Gaspar, A.B. Cyclohexene to adipic acid synthesis using heterogeneous polyoxometalate catalysts. *Mol. Catal.* **2018**, *458*, 223–229. [[CrossRef](#)]
57. Alcañiz-Monge, J.; Trautwein, G.; Garcia-Garcia, A. Influence of peroxometallic intermediaries present on polyoxometalates nanoparticles surface on the adipic acid synthesis. *J. Mol. Catal. A* **2014**, *394*, 211–216. [[CrossRef](#)]
58. Predoeva, A.; Damyanova, S.; Gaigneaux, E.M.; Petrov, L. The surface and catalytic properties of titania-supported mixed PMoV heteropoly compounds for total oxidation of chlorobenzene. *Appl. Catal. A* **2007**, *319*, 14–24. [[CrossRef](#)]
59. Maestre, J.M.; Lopes, X.; Bo, C.; Poblet, J.-M.; Casoñ-Pastor, N. Electronic and magnetic properties of  $\alpha$ -Keggin anions: A DFT study of  $[\text{XM}_{12}\text{O}_{40}]^{n-}$ , ( $\text{M} = \text{W}, \text{Mo}$ ;  $\text{X} = \text{Al}^{\text{III}}, \text{Si}^{\text{IV}}, \text{P}^{\text{V}}, \text{Fe}^{\text{III}}, \text{Co}^{\text{II}}, \text{Co}^{\text{III}}$ ) and  $[\text{SiM}_{11}\text{VO}_{40}]^{m-}$  ( $\text{M} = \text{Mo}$  and  $\text{W}$ ). *J. Am. Chem. Soc.* **2001**, *123*, 3749–3758. [[CrossRef](#)]
60. Ali, B.E.; El-Ghanam, A.M.; Fettouhi, M.  $\text{H}_{3+n}\text{PMo}_{12-n}\text{V}_n\text{O}_{40}$ -catalyzed selective oxidation of benzoin to benzil or aldehydes and esters by dioxygen. *J. Mol. Catal. A* **2001**, *165*, 283–290. [[CrossRef](#)]
61. Ballarini, N.; Casagrandi, L.; Cavani, F.; D’Alessandro, T.; Frattini, A.; Accorinti, P.; Alini, S.; Babini, P. The liquid-phase oxidation of cyclohexanone with oxygen, catalysed by Keggin-type polyoxometalates. A cleaner alternative to the current industrial process for adipic acid synthesis. In *Book of Abstracts Convegno Nazionale Chimica Verde Chimica Sicura*; Università degli Studi di Pavia e GI Green Chemist: Pavia, Italy, 2008; pp. 225–232.

**Disclaimer/Publisher’s Note:** The statements, opinions and data contained in all publications are solely those of the individual author(s) and contributor(s) and not of MDPI and/or the editor(s). MDPI and/or the editor(s) disclaim responsibility for any injury to people or property resulting from any ideas, methods, instructions or products referred to in the content.